The Effect of Ce and Nd Addition on Dry/Corrosive Wear Behavior of Newly Developed EZ43 Grade Mg Alloys

Özcan BÜYÜKGENÇ [1] *, Hayrettin AHLATCI [1], Yunus TÜREN [2], İsmail ESEN [3]

[1] *Karabuk University Central Campus, Faculty of Engineering, Metallurgical and Materials Engineering, 78050, Karabuk, Turkey*
[2] *Necmettin Erbakan University, Machine Engineering, Köyceğiz Mah. Demeç Sok. No:44/1, 42090 Meram/Konya, Turkey*
[3] *Karabuk University, Central Campus, Faculty of Engineering, Mechanical Engineering, 78050, Karabuk, Turkey*

http://doi.org/10.5755/j02.ms.37901

Received 9 July 2024; accepted 4 November 2024

This study is concerned with the production of EZ43A and EZ43B alloys by induction melting/casting method and their microstructure, mechanical, and dry/corrosive wear properties. The investigated EZ43A and EZ43B alloys were alloyed with 1 % Ce – 2 % Nd and 2 % Ce – 1 % Nd, respectively. According to the XRD results, ternary Mg0.97Zn0.03/Mg41Nd5/Mg3Gd eutectic phases were present in the microstructure of EZ43A alloy, while quaternary Mg0.97Zn0.03/Mg41Nd5/Mg3Gd/Mg17Ce2 eutectic phase was formed in the microstructure of EZ43B alloy. The hardness increased from 60.41 to 63.34 by increasing Ce from 1 % to 2 %, representing a 5 % improvement in hardness. As the Ce/Nd ratio increased, the yield/tensile strength and modulus of elasticity increased by 2 %, 6 %, and 3 %, respectively. With the increase in Ce, the relative dry wear loss of EZ43A was 1.00, while that of EZ43B was 0.93, and the corrosive relative wear loss of EZ43A was 2.44 and that of EZ43B was 1.56. Accordingly, the dry and corrosive wear resistance of EZ43B increased by 7 % and 36 %, respectively, compared to that of EZ43A.
Keywords: EZ43, extrusion, microstructure, strength, wear, homogenization.

1. INTRODUCTION

Due to the developments in today's technologies and the emergence of different needs in our lives, the need to develop new materials with superior properties to the currently used materials and the traditionally used materials is increasing day by day. In line with this increasing need, materials produced by researchers in the form of composites, which have the best properties of two or more materials and are described as hybrid materials, are being produced and studies proceed in this direction.

One of these studies and research is on Magnesium and magnesium alloys. Magnesium is the lightest element among other constructive metals in terms of density, with a density of 1.74 g/cm^3. Therefore, there is an increasing interest in magnesium and its alloys due to this feature in studies where lightness is at the forefront [1, 2]. Magnesium alloys, which create an increasing interest in energy, have an increasing importance in fields such as automotive, aerospace, construction, and sports equipment, as well as electronics and other consumer products [3, 4]. Rare earth (RE) elements are traditionally used to improve mechanical properties in Mg alloys [5].

In magnesium and its alloys, Cerium (Ce), Lanthanum (La), Neodymium (Nd), Thorium (Th), Yttrium (Y), Gadolinium (Gd) and Scandium (Sc) are rare earth elements (RE) that provide a wide range of use is counted [6].

The addition of cerium (Ce) and Neodymium (Nd) to magnesium alloys has been extensively studied for their effects on the microstructure and mechanical properties of the alloys. Numerous studies have shown that the addition of rare earth elements, including Ce and Nd, can indeed improve the mechanical properties of magnesium alloys [7 – 13]. These improvements include increased tensile strength, yield strength, and elongation, as well as enhanced high-temperature properties. The addition of Nd has been found to refine the microstructure of magnesium alloys, decrease the size of precipitating phases, and increase the volume fraction of certain phases [8, 10, 14]. It has also been observed that the addition of Ce and Nd can enhance the corrosion resistance of magnesium alloys [9, 15, 16]. However, it should be noted that excessive addition of Ce or Nd could lead to reduced ductility and excessive surface oxidation during extrusion [7]. Overall, the addition of Ce and Nd to magnesium alloys has shown promise in improving their mechanical properties and corrosion resistance, making them suitable for various applications, including automotive and biomedical applications [8, 10, 14, 17 – 22].

Mg alloys have been a promising material in the use of aircraft engines, helicopter gearboxes, vehicles that require high performance and in the production of biomedical materials, as well as commercial applications, as the presence of alloying elements produced by casting method increases strength and ductility [23, 24].

In addition, wrought magnesium alloys prepared by conventional thermomechanical processes such as extrusion, rolling, or forging have received considerable attention in the load-bearing range of applications [5].

It is evaluated that these new materials can be used as an alternative material to biocompatible materials. In addition, it is considered an alternative material resistant to

* Corresponding author: O. Büyükgenç
E-mail: *buyukgencozcan@karabuk.edu.tr*

thermal creep in space and aviation applications such as high-temperature applications, engines, and transmission bodies, and can be used in the production of light structural parts in the automotive industry, defense industry, armored vehicles, or military aircraft.

Although there are limited studies on EZ33 alloys [25] in the literature and no studies on EZ43 alloys, EZ43, which is the purpose of this paper, is a brand-new alloy. Only Rogal et al. [25] investigated the effect of grain size and ageing heat treatment on the mechanical properties of EZ33 alloy produced by Thixo-Cast containing 1.2 Ce and 0.9 Nd. In this study, two new materials named EZ43A and EZ43B containing (1 % and 2 % Ce and (2 % and 1 % Neodymium) were produced for the first time by induction melting under a protective atmosphere and microstructure, tensile, hardness, dry environment and corrosive environment (Hank's Balanced Salt Solution) wear properties were investigated. The investigated EZ43A/EZ43B alloys were found to have improved wear resistance and corrosion behaviour than that of the EZ33 alloy.

It is evaluated that these new materials can be used as an alternative material to biocompatible materials. It is also evaluated as an alternative material resistant to thermal creep in space and aviation applications, high temperature applications, engines and transmission organs, and can be used in the production of lightweight structural parts in the automotive industry, defense industry, armored vehicles or military aircraft.

2. MATERIALS AND METHOD

In the preparation of EZ43 magnesium alloys for experimental studies, commercial grade Mg (99.7 %) and high purity (99.9 %) Zn were obtained, and Neodymium, Cerium, Gadolinium, Zirconium, and Calcium, which were supplied as master alloys, were used. Before the casting process, a ceramic casting filter was placed at the end of the runner and the alloy was filtered through this strainer and filled into the mold. Thus, the produced alloy with minimal inclusions was included. Atmosphere-controlled induction casting furnace was used in the melting and casting processes of the alloys.

In this method, first, Mg ingots were placed in the crucible and melted at approximately 750 °C, then zinc, neodymium, cerium, gadolinium, zirconium, and calcium elements were added to the molten metal. After keeping the melt at this temperature for 30 minutes and applying mechanical mixing for 20 minutes, it was filled into the steel mold, whose mold temperature was determined as approximately 270 °C, under gas (CO_2+1SF6) protection. Amounts of the elements by weight of the EZ43A and EZ43B alloy after XRF are given in Table 1.

Table 1. Element amounts by wt.% in EZ43A and EZ43B alloys

Alloys	Mg	Zn	Nd	Ce	Gd	Zr	Ca
EZ43A	92	3	2	1	1	0.5	0.5
EZ43B	92	3	1	2	1	0.5	0.5

Homogenization heat treatment was applied to all alloys before extrusion to ensure that micro segregations that may occur in the structure after casting and secondary phases with low thermal stability, which may cause problems during extrusion, are dissolved in the matrix phase. After the cast ingots were tightly wrapped with aluminum foil, they were buried in a SiO_2+Graphite sand mixture and kept at 400 °C for 24 hours. To preserve the homogenized structure, the samples removed from the furnace were kept in the open air and cooled.

The homogenization process was completed and the alloys were extruded with a hydraulic press. Before extrusion, first, the billet, die, and punch are lubricated with a heat-resistant Molykote brand, MoS_2-based spray lubricant. The extrusion of the alloys was done with the assistance of a hydraulic press with a capacity of 30 tons. Extrusion molds were heated with clamp resistances, and temperature control was provided by the unit connected to the press. The extrusion process of the alloy was carried out at a temperature of about 350 °C and a speed of 0.3 mm/s. To distribute homogeneous temperature throughout the billet, the alloys, which reached the required temperature for the extrusion process, were kept in the heat treatment furnace for 2 hours. After reaching the desired extrusion temperature, extrusion samples with a length of 10 × 110 mm were obtained after the extrusion by moving the punch connected to the press and applying pressure to the cylindrical billet with a diameter of 32 mm and a length of 60 mm in the mold. As a result, the calculated 7:1 extrusion ratio was used in this study. The low extrusion rate used is a preparatory step in obtaining the required sample shape for the next test.

Standard metallographic processes were applied to the alloy samples obtained after extraction, and microstructure examinations were carried out for investigations by taking SEM images in a Scanning Electron Microscope (SEM) device, EDX and elemental mapping (MAP) analyses were performed. Five dog-bone-shaped tensile samples measuring 30 mm × 5 mm were prepared from extruded EZ43A and B alloys. The tensile tests of the samples were carried out on a Shimadzu brand tensile device that can be adjusted to 5 tons of tensile capacity at a tensile speed of 1 mm/min. The hardness of the samples was determined by the Brinell hardness test in BMS 3000-HB BRINELL Hardness Tester. The hardness test was carried out under a load of 750 kgf with a ball diameter of 5 mm for 10 seconds. The samples were removed from the centers of the extruded alloy in dimensions of 20 × 20 × 20 mm and their surfaces were polished by sanding. While applying the hardness test to the samples, at least three different points were determined at equal intervals from the outermost point of the sample to its center, hardness measurements were made from these determined points, and the values were averaged.

Wear tests were carried out in two different environments, a dry environment and a corrosive environment. In both wear methods, a load of 20 Newtons was used and it was carried out at a sliding speed of 0.48 m/minute at a total sliding distance of 400 m at 100 m intervals. A 6 mm diameter 100Cr6 quality steel ball was used as the counter surface in the wear tests. Before the test, the sample surfaces were sanded with 400 – 1200 grit sandpaper and cleaned with alcohol.

In the wear tests, the weights were measured on a digital precision balance with an accuracy of 0.1 mg after each 100 meter sliding distance. Before measuring the weight loss on a precision balance, the sample was cleaned with distilled water and methyl alcohol and dried with a dryer,

then weight loss measurements were carried out. The data obtained as a result of the measurement were recorded and weight loss graphs were drawn according to the sliding distance. In the abrasive wear test, the samples and steel shot were together in Hank's Balanced Salt Solution its acidity level 7.4 pH, NaCl 8.0 g/l, KCl 0.4 g/l, $CaCl_2$ 0.14 g/l, $NaHCO_3$ 0.35 g/l, $C_6H_6O_6$ (glucose) 1.0 g/l, $MgCl_2$ $6H_2O$ 0.1 g/l, $MgSO_4$ $7H_2O$ 0.06 g/l, KH_2PO_4 0.06 g/l, Na_2HPO_4 $12H_2O$ 0.06 g/l. After the wear tests, detailed SEM and elemental mapping (MAP) analyses were performed to determine the wear mechanisms of the alloys.

3. RESULTS AND DISCUSSION

Optical microstructure and SEM images of the EZ43A and B alloys are given in Fig. 1. A coaxial grain structure and intermetallic phases extending continuously at grain boundaries, as well as eutectic structures created by mixed intermetallics, are found in the microstructures of the EZ43A and B alloys. Intermetallics observed at the grain boundaries are light gray in EZ43A and dark in EZ43B. EZ43A alloy is coarser than EZ43B alloy. The grain size of the EZ43B alloy is 8.52 µm, while the grain size of the EZ43A alloy is 9.01 µm.

Rogal et al. [25] investigated the effect of aging on the grain size of the Thixo-Cast EZ33 alloy containing 1.2 Ce and 0.9 Nd and reported that the grain size of Thixo-Cast EZ33 alloy increased by 92 µm and aging. Compared to the work of Rogal et al. [25], the grain size of the EZ43A and B alloys is quite refined. This can be attributed to the extrusion process applied to EZ43 A and B alloys and the high amount of Ce and Nd contained in the alloy. The grain size of the EZ43B alloy is finer than that of the EZ43A alloy, due to the excess Ce content it contains. In addition, Tong et al. [5] reported similar results in their studies on the microstructure, mechanical properties, and corrosion resistance of extruded Mg-Zn-Ca xCe/La. The XRD response spectrum results showing the phase compositions of the investigated EZ43A and B alloys are given in Fig. 2. The XRD results of the EZ43A and B alloys in Fig. 2 show that α-Mg, Mg0.97Zn0.03, Mg41Nd5, Mg17Ce2, Mg2Ca, Mg3Gd, and Zr intermetallic phases are observed. The differences in the chemical composition of the EZ43A and B alloys (Table 1) have not changed the number and type of phases formed, except for the grain size (Fig. 1).

The EDX analysis of the EZ43A and B alloys, whose SEM images are given in Fig. 1, are listed in Table 2. The more intense intermetallic formation was determined in the EZ43B alloy compared to the EZ43A alloy from SEM images and EDX analysis results. High concentrations of alloying elements were observed, suggesting the presence of eutectic mixing and complex intermetallic phases.

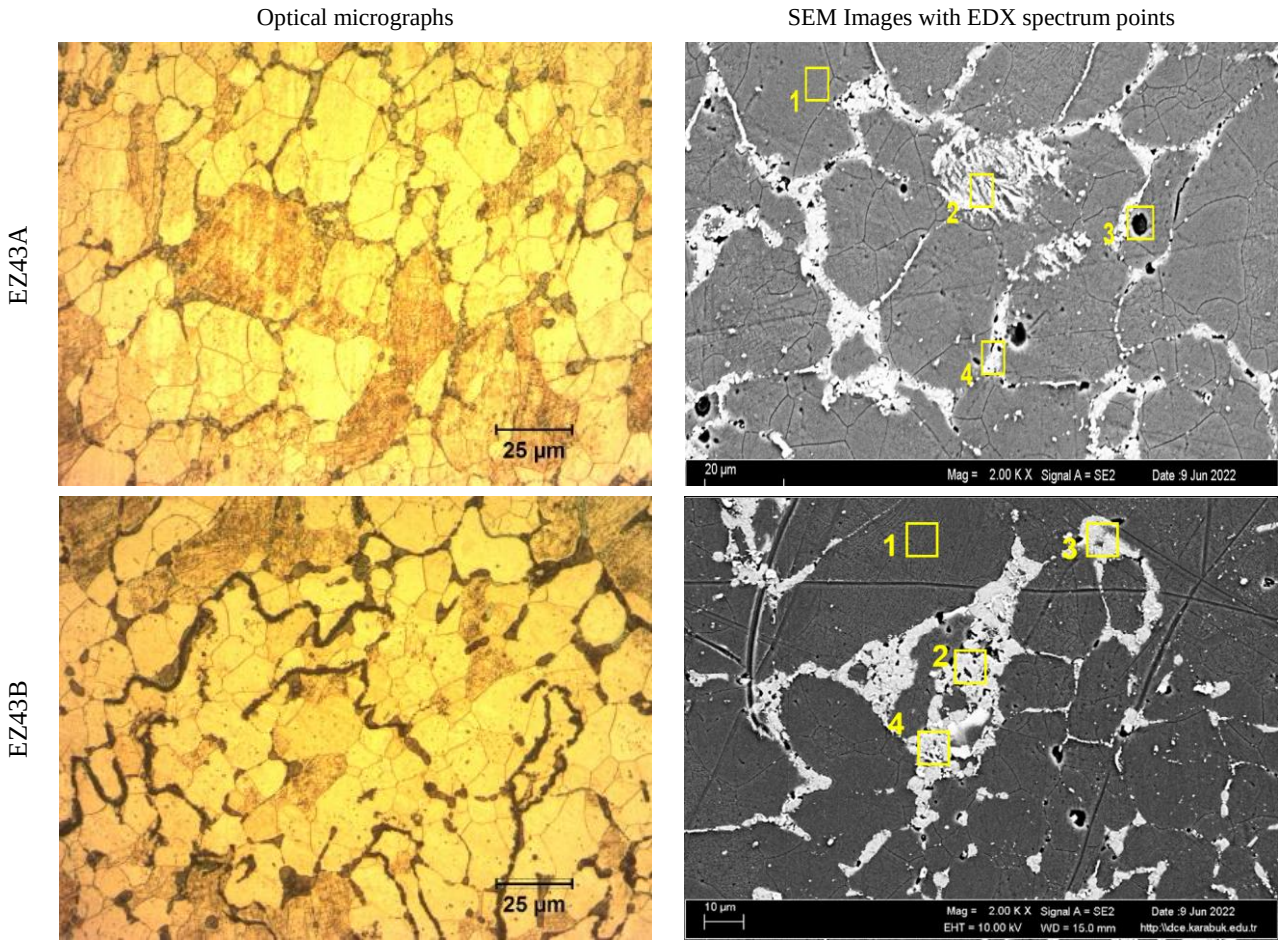

Fig. 1. Optical micrographs (50^X magnification) and SEM images ($2K^X$ magnification) of the EZ43A and EZ43B alloys

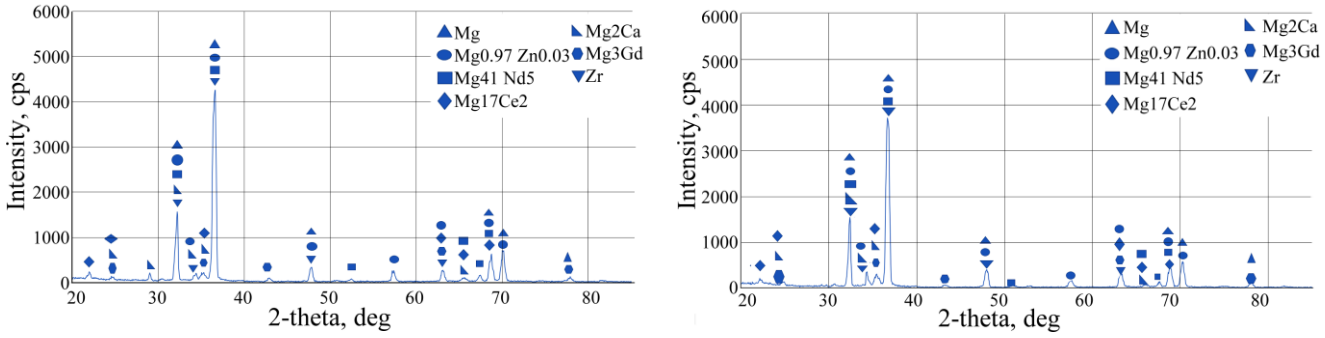

Fig. 2. XRD elemental response spectrum results: a – EZ43A; b – EZ43B alloys

Table 2. EDX spectrum results of selected areas in the SEM image of the EZ43A and EZ43B alloys

Samples	Mass %							
	Spc.	Mg	Ca	Zn	Zr	Ce	Nd	Gd
EZ43A	1	72.90	0.047	1.06	0.23	0.072	0.19	25.61
	2	56.99	0.40	5.72	12.00	0.71	1.96	22.21
	3	58.56	0.28	5.48	10.48	0.54	2.81	21.86
	4	55.97	0.88	10.82	0.00	3.78	6.04	22.52
EZ43B	1	72.92	0.20	1.09	0.08	0.05	0.00	25.64
	2	54.59	0.53	12.28	0.00	7.93	3.62	21.03
	3	42.89	0.42	19.13	0.06	12.1	5.94	19.35
	4	26.71	0.45	33.58	0.00	3.05	14.07	22.14

The EDX analysis results given in Table 2 show that regions numbered 1 are α-Mg matrices and dissolve Gd in its structure. In addition, EDX analysis results of areas 2 – 4 show that a ternary eutectic structure is formed from Mg0.97Zn0.03/Mg41Nd5/Mg3Gd mixed intermetallics at the grain boundaries of EZ43A alloy, while Mg0.97Zn0.03/Mg41Nd5/Mg3Gd/Mg17Ce2 quaternary eutectic structure is formed at the grain boundaries of EZ43B alloy. EDX analysis of points 2 – 4 marked in the microstructure of EZ43A alloy (Table 2) revealed that it is rich in Zn, Ndm and Gd elements, thus ternary eutectic phase Mg0.97Zn0.03, Mg41Nd5 and Mg3Gd mixed intermetallics are formed at grain boundaries. According to the EDX analysis results (Table 2), the quaternary eutectic phases formed in the grain boundaries of the EZ43B alloy were rich in Zn, Nd, Gd, and Ce elements, causing the formation of the quaternary eutectic Mg0.97Zn0.03/Mg41Nd5/Mg3Gd/Mg17Ce2 structure.

4. MECHANICAL PROPERTIES

The hardness, yield/tensile strengths, and modulus of elasticity values acquired from the stress-strain diagrams are given in Table 3. As a result of the hardness test of the extruded EZ43 alloys, the average hardness values shown in Table 3 were obtained. While the hardness value of EZ43A alloy is 60.41 HB, the hardness value of EZ43B alloy is 63.34 HB. The difference is small and can be attributed to the formation of a low amount of resistance against the sinking of the penetrating tip, due to the intense intermetallic phases formed at the grain boundaries of the EZ43B alloy with the increase of Ce. According to these results given in Table 3, it is seen that the yield strength of the EZ43A alloy with a Ce/Nd ratio of 0.5 is 199.18 MPa, while the yield strength of EZ43B alloy with a Ce/Nd ratio of 2 is 202.88 MPa. It is also seen that the tensile strength of the EZ43A alloy is 242.30 MPa, and the EZ43B alloy is 257.13 MPa. When we look at the elastic modulus, it is seen that the elastic modulus of the EZ43A alloy is 103.13 GPa, and the B alloy is 115.80 GPa. As the Ce/Nd ratio increased in the examined alloys, it was observed that the strength properties of the EZ43B alloy slightly increased due to the increase in the Mg0.97Zn0.03/Mg41Nd5/Mg3Gd/Mg17Ce2 quaternary eutectic structure. The findings of Rogal et al. [25] and Tong et al. [5] were similar to those of this investigation. Tong et al. [5] reported that the tensile test properties increased up to 0.5 Ce/La ratio and the strength decreased with the addition of 1 Ce/La ratio. In this study, while the maximum ratio of Ce/Nd added was 2 it showed an improvement of 5 % in the hardness of the formed eutectic intermetallics. Compared to the EZ43A alloy, the increase in the Ce/Nd ratio to 2 in the EZ43B alloy resulted in denser grain boundary quaternary eutectic phases (Fig. 1) leading to grain boundary strengthening, which exhibited improved mechanical properties.

Table 3. Hardness, yield-tensile strength, and modulus of elasticity values of EZ43 alloys

No	Samples	Average hardness, HB	Modulus of elasticity, GPa	%0.2 Yield strength, MPa	Tensile strength, MPa
1	EZ43A	60.41	103.13 ± 7.21	199.18 ± 18.98	242.30 ± 10.2
2	EZ43B	63.34	115.80 ± 8.70	202.88 ± 15.55	252.13 ± 10.7

5. WEAR TESTS

Two different wear tests, dry and corrosive, were applied to the EZ43A and B alloys, and the wear test results are given in Fig. 3 a and Fig. 3 b, respectively. It is seen that the weight loss values of the EZ43A sample with 1 % Ce added in both dry environment and corrosive environment wear test are higher than those of the EZ43B sample added to 2 % Ce. As seen in the dry wear results of the extruded EZ43A and EZ43B alloys, the EZ43A sample wears 7.8 % more than the EZ43B sample. In addition, corrosive media weight losses are significantly higher than dry media weight losses. The EZ43A specimen wore 144 % more in a corrosive environment compared to a dry environment. The EZ43B specimen, on the other hand, wore 68 % more in the corrosive environment compared to the dry environment. When the corrosive wear results of the examined samples were examined within themselves, it was seen that the EZ43A alloy showed 56 % more corrosion in the corrosive environment than the EZ43B alloy.

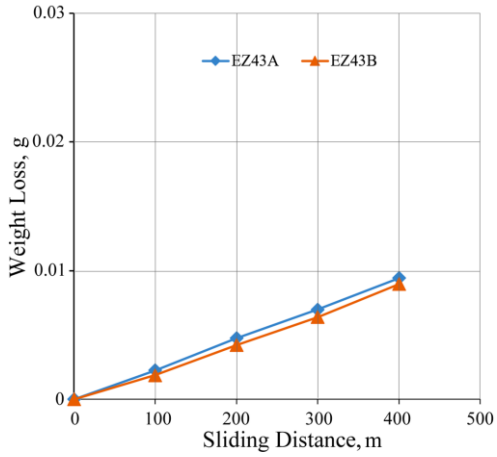

a

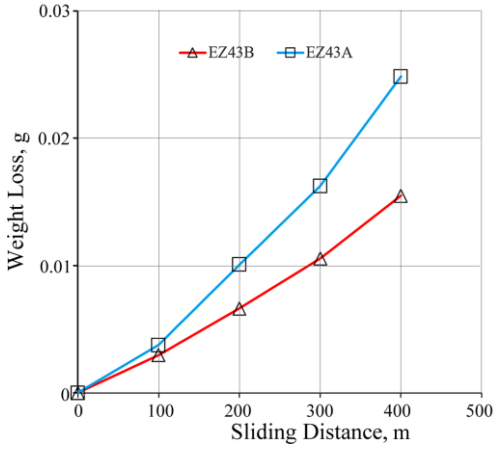

b

Fig. 3. Wear test results of EZ43A and EZ43B alloys in: a – a dry environment; b – a corrosive environment

The slope of the weight loss-sliding distance curves shown in Fig. 3 gives the wear rate in g/m, and the change in wear rates of the examined alloys is displayed in Fig. 4. Fig. 4 provides evidence that dry wear rates are lower than corrosive medium wear rates and that EZ43B wear rates are lower than EZ43A wear rates.

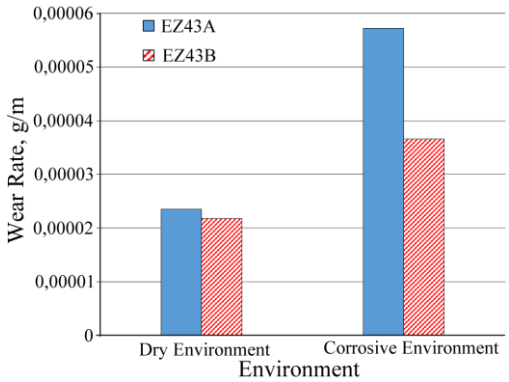

Fig. 4. Variation of wear rates of the studied alloys.

By using the wear rate data of the examined alloys given in Fig. 4, the wear coefficient of the EZ43A alloy, which was abraded in dry conditions, is taken as 1, and the comparison of the relative wear behavior of the others is given in Table 4. According to Table 4, in the case of adding 1 % Ce to EZ43A alloy and reducing 1 % Nd (EZ43B), the dry environment wear coefficient decreased to 0.93. By increasing Ce to 2 and decreasing the Nd amount to 1 % (EZ43B), the corrosive environment wear coefficient decreased to 1.56 again. The corrosive environmental wear coefficient of EZ43A alloy containing 1 % Ce and 2 % Nd reached the highest value of 2.44. It is thought that the better wear resistance of the examined EZ43B, compared to that of the EZ43A samples, is due to the density of the quaternary eutectic intermetallic phases formed in the structure by more added Ce.

Table 4. Comparison of the relative wear behavior of the examined alloys

Environments	Alaşım Tipi	Relative wear behavior
Dry	EZ43A	1.00
	EZ43B	0.93
Corrosive	EZ43A	2.44
	EZ43B	1.56

SEM images of EZ43A and B samples after dry and corrosive wear tests are given in Fig. 5. The dry environment SEM images given in Fig. 5 show that the wear develops with the formation of grooves and the presence of rough areas adhered to the surface is observed in the SEM image of the EZ43B alloy compared to the worn surface appearance of the EZ43A. The SEM image with a rough, worn surface indicates the presence of an adhesion wear mechanism, while the smooth grooved surface (SEM image of the EZ43A alloy) indicates the presence of an abrasive wear mechanism. Fig. 6 shows the element mapping analysis result of the dry worn surfaces of the alloys studied. As seen in Fig. 6, the fact that the oxygen-rich regions of the EZ43B alloy are denser on the worn surface indicates that the oxidized film adheres to the surface, while the worn surface MAP analysis of EZ43A shows the Mg element distribution rather than the oxide film, which shows that the main matrix structure constantly comes to the surface during wear. When the corrosive media worn surface images of the alloys are examined (Fig. 5), it is seen that alloy A exhibits a flat, shiny surface, and alloy B has a rough surface after wear tests. Tong et al. [5] investigated the corrosion behavior of Mg-Zn-Ca alloy with the addition of Ce and

reported that an oxide film was formed on the surface with the addition of 0.5 % Ce and accelerated the corrosion behavior of cracks and cavities formed with this oxide film. It is thought that the appearance of spherical and adhered particles on the worn surface of the EZ43B alloy containing 2 % Ce given in Fig. 5 causes an oxide layer to remain on the surface with the applied load of the corrosion products formed during the wear. This significantly improved the wear resistance of EZ43B alloy in a corrosive environment compared to a dry environment.

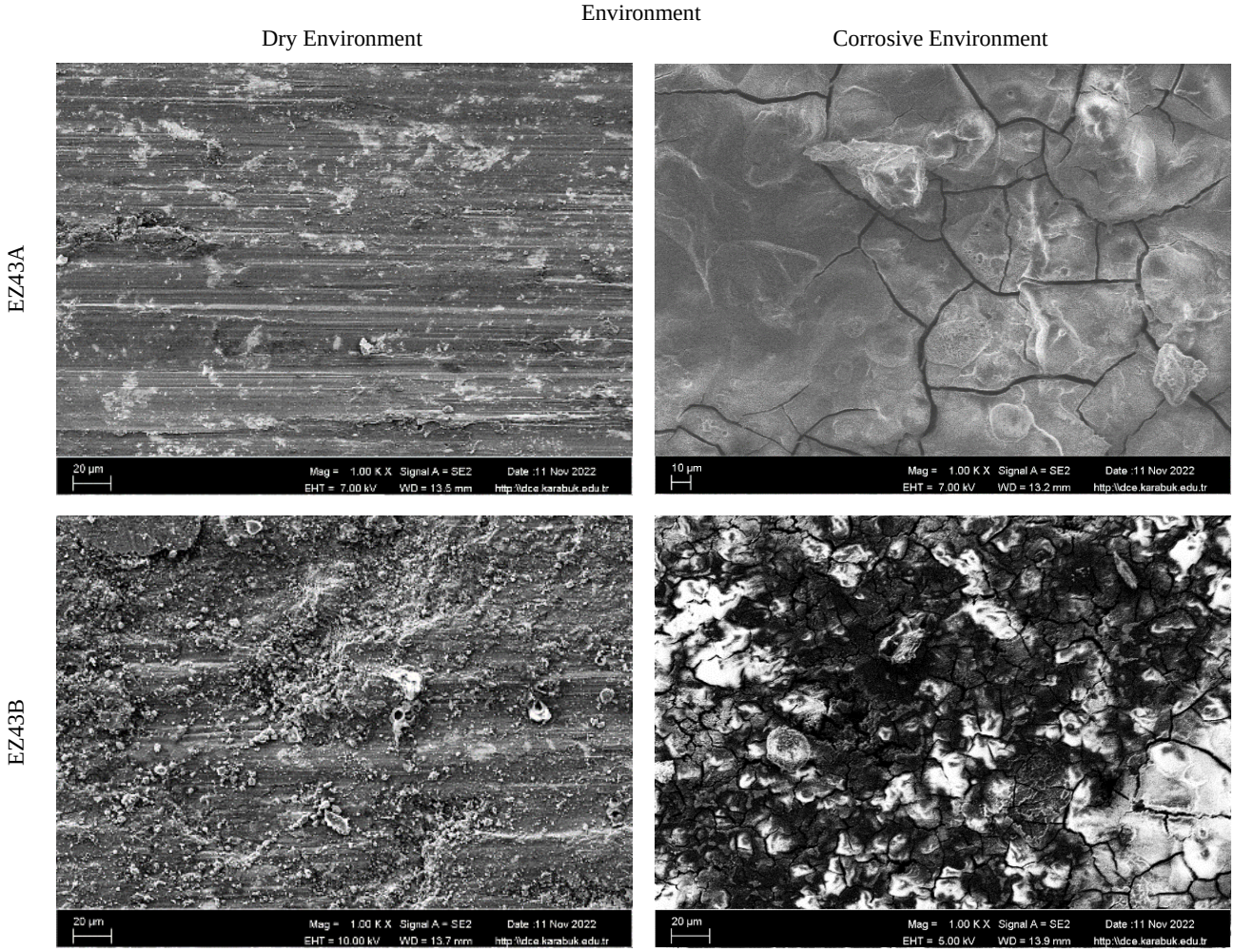

Fig. 5. SEM images (1kx) of EZ43A and EZ43B alloys after dry and corrosive wear test

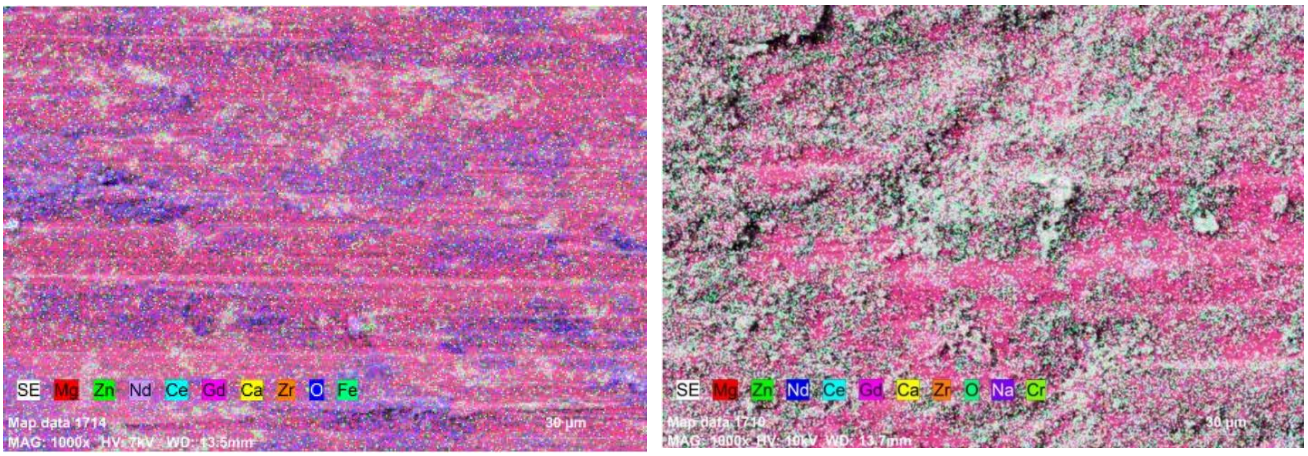

a b

Fig. 6. Elemental mapping analysis image: a – EZ43A; b – EZ43B alloys dry weathered surfaces (1kx)

6. CONCLUSIONS

The general results obtained from this study, in which the microstructure, mechanical and dry/corrosive environment wear behaviors of EZ43A containing 1 % Ce, 2 % Nd and EZ43B alloy containing 2 % Ce, 1 % Nd were examined, are summarized below.

1. EZ43A alloy has a coarser grain than EZ43B alloy. The grain size of the EZ43B alloy is 8.52 μm, while the grain size of the EZ43A alloy is 9.01 μm.
2. As examined the XRD results of the EZ43A and B alloys, α-Mg, Mg0.97Zn0.03, Mg41Nd5, Mg17Ce2, Mg2Ca, Mg3Gd and Zr intermetallic phases are observed. The differences in the chemical composition of the EZ43A and B alloys did not change the number and type of phases formed, except for grain size.
3. The EDX analysis results of the alloys show that a ternary eutectic structure is formed from Mg0.97Zn0.03/Mg41Nd5/Mg3Gd mixed intermetallics at the grain boundaries of the EZ43A alloy, while the Mg0.97Zn0.03/Mg41Nd5/Mg3Gd/ Mg17Ce2 quaternary phases is formed at the grain boundaries of the EZ43B alloy.
4. As the Ce/Nd ratio increased, the yield and tensile strength improved by 2 % and 6 %, respectively. The increase in the modulus of elasticity is 3 %. The addition of 2 % Ce led to a 5 % improvement in hardness due to the intermetallics formed.
5. The dry environment wear behavior of the EZ43A alloy (containing 1 % Ce and 2 % Nd) was 7.8 % more severe than that of the EZ43B (alloyed by 2 % Ce and 1 % Nd). In the corrosive environment wear test, decreasing the Nd content to 1 % (EZ43B) reduced the amount of wear by 56 %.

Acknowledgements

This study is derived from the PhD thesis of Özcan Büyükgenç at the Karabük University Institute of Graduate Programs (KBÜBAP-24-DS-144).

REFERENCES

1. **Song, G., Song, S.** A Possible Biodegradable Magnesium Implant Material *Advanced Engineering Materials* 9 (4) 2007: pp. 298 – 302. https://doi.org/10.1002/adem.200600252
2. **Zheng, Y.F., Gu, X.N., Witte, F.** Biodegradable Metals *Materials Science and Engineering: R: Reports* 77 2014: pp. 1 – 34. https://doi.org/10.1016/j.mser.2014.01.001
3. **Chen, Y., Xu, Z., Smith, C., Sankar, J.** Recent Advances on the Development of Magnesium Alloys for Biodegradable implants *Acta Biomaterialia* 10 (11) 2014: pp. 4561 – 4573. https://doi.org/10.1016/j.actbio.2014.07.005
4. **Staiger, M.P., Pietak, A.M., Huadmai, J., Dias, G.** Magnesium and Its Alloys as Orthopedic Biomaterials: A Review *Biomaterials* 27 (9) 2006: pp. 1728 – 1734. https://doi.org/10.1016/j.biomaterials.2005.10.003
5. **Tong, L.B., Zhang, Q.X., Jiang, Z.H., Zhang, J.B., Meng, J., Cheng, L.R., Zhang, H.J.** Microstructures, Mechanical Properties and Corrosion Resistances of Extruded Mg–Zn–Ca–xCe/La Alloys *Journal of the Mechanical Behavior of Biomedical Materials* 62 2016: pp. 57 – 70. https://doi.org/10.1016/j.jmbbm.2016.04.038
6. **Purnama, A., Hermawan, H., Couet, J., Mantovani, D.** Assessing the Biocompatibility of Degradable Metallic Materials: State-of-the-art and Focus on the Potential of Genetic Regulation *Acta Biomaterialia* 6 (5) 2010: pp. 1800 – 1807. https://doi.org/10.1016/j.actbio.2010.02.027
7. **Luo, A., Wu, W., Mishra, R., Jin, L., Sachdev, A., Ding, W.** Microstructure and Mechanical Properties of Extruded Magnesium-aluminum-cerium Alloy Tubes *Metallurgical and Materials Transactions A* 41 (10) 2010: pp. 2662 – 2674. https://doi.org/10.1007/s11661-010-0278-3
8. **Hamzah, M., Ahmad, R., Asmael, M., Sheggaf, Z.** Effects of Rare Earth Neodymium on Microstructure and Mechanical Properties of Mg-Ce-Zn-Zr alloy *International Journal of Materials Science and Engineering* 5 (4) 2017: pp. 133 – 139. https://doi.org/10.17706/ijmse.2017.5.4.133-139
9. **Li, Q., Zhu, W., Zeng, B., Jiang, X.** Effect of Ce on Deformation Performance of ZK20 Magnesium Alloy *6th International Conference on Mechatronics, Materials, Biotechnology and Environment (ICMMBE 2016)* 2016: pp. 59 – 63. https://doi.org/10.2991/icmmbe-16.2016.13
10. **Jinwang, Z., Shebin, W., Jun-yuan, Z., Jinling, Z., Bingshe, X.** Effects of Nd on Microstructures and Mechanical Properties of AM60 Magnesium Alloy in Vacuum Melting *Rare Metal Materials and Engineering* 38 (7) 2009: pp. 1141 – 1145. https://doi.org/10.1016/s1875-5372(10)60044-6
11. **Wang, J., Wang, L., An, J., Liu, Y.** Microstructure and Elevated Temperature Properties of Die-cast AZ91-xNd Magnesium Alloys *Journal of Materials Engineering and Performance* 17 (5) 2008: pp. 725 – 729. https://doi.org/10.1007/s11665-007-9168-2
12. **Li, Q., Zhu, W., Jiang, X., Zeng, B., Pan, F.** Effects of Ce and Homogenizing on Microstructure and Mechanical Properties of ZM21 Magnesium Alloy *5th Int. Conf. on Information Engineering for Mechanics and Materials (ICIMM 2015)* 2015: pp. 1741 – 1744. https://doi.org/10.2991/icimm-15.2015.325
13. **Li, Q., Zhu, W., Jiang, X., Zeng, B., Pan, F.** Effects of Nd on Extrusion Microstructure and Mechanical Properties of ZK20 Magnesium Alloy *5th International Conference on Information Engineering for Mechanics and Materials (ICIMM 2015)* 2015: pp. 1745 – 1748. https://doi.org/10.2991/icimm-15.2015.326
14. **Yan, J., Li, Q., Zhang, X., Zhou, Y.** Effects of Nd on Microstructure Mechanical Properties of Mg-10Gd-3y-0.5Zr Alloy *International Conference on Material Science and Civil Engineering (MSCE 2016)* 2016: pp. 294 – 300. https://doi.org/10.12783/dtmse/ msce2016/10484
15. **Liu, X., Jia, R., Fu, X., Cheng, W., Zhang, H., Zhao, E.** First-principles Calculation and Experimental Study on the Effect of Rare Earth Ce and Nd on the Corrosion Behavior of Mg Alloys *Materials Research Express* 10 2023: pp. 026513. https://doi.org/10.1088/2053-1591/acbae5
16. **Ning, F., Le, Q., Kong, S.** Effect of Annealing Temperature on Corrosion Properties of Rolled AZ31-Ce Magnesium Alloy *Sn Applied Sciences* 2 (762) 2020: pp. 1 – 8. https://doi.org/10.1007/s42452-020-2398-8

17. **Drynda, A., Deinet, N., Braun, N., Peuster, M.** Rare Earth Metals Used in Biodegradable Magnesium-based Stents Do Not Interfere with Proliferation of Smooth Muscle Cells but Do Induce the Upregulation of Inflammatory Genes *Journal of Biomedical Materials Research Part A* 91A (2) 2009: pp. 360 – 369. https://doi.org/10.1002/jbm.a.32235
18. **Wang, Z., Wang, J., Chen, Z., Zha, M., Wang, C., Liu, S., Yan, R.** Effect of Ce addition on Modifying the Microstructure and Achieving a High Elongation with a Relatively High Strength of As-extruded AZ80 Magnesium Alloy *Materials* 12 (1) 2019: pp. 1 – 12. https://doi.org/10.3390/ma12010076
19. **Guo, H., Liu, S., Huang, L., Wang, D., Du, Y., Chu, M.** Thermal Conductivity of As-cast and Annealed Mg-Re Binary Alloys *Metals* 11 (4) 2021: pp. 1 – 12. https://doi.org/10.3390/met11040554
20. **Jia, Y., Sun, W., Xiao, Y., Liu, Y., Tian, S.** Effect of Rare Earth on the Corrosion Resistance of Electroless Ni-Mo-P Composite Coatings *Materials Research* 25 2022: pp. 1 – 14. https://doi.org/10.1590/1980-5373-mr-2021-0278
21. **Stulíková, I., Smola, B., Mordike, B.** New High Temperature Creep Resistant Mg-Ynd-Sc-Mn alloy *Physica Status Solidi (A)* 190 (2) 2022: pp. 5 – 7.
22. **Dai, F., Cheng, X., Rong, M., Yao, Q., Wang, J.** Phase Formation and Magnetic Properties of La- and Ce-substituted $(Nd_{1-2x}RE_xPr_x)_{2.28}Fe_{13.58}B_{1.14}$ Melt-Spun Ribbons *Physica Status Solidi (A)* 218 (21) 2021: pp. 1 – 5. https://doi.org/10.1002/pssa.202100371
23. **Zheng Y.** Magnesium Alloys as Degradable Biomaterials. CRC Press, 2015. https://doi.org/10.1201/b18932
24. **Tie, D., Feyerabend, F., Müller, W.D., Schade, R., Liefeith, K., Kainer, K., Willumeit, R.** Antibacterial Biodegradable Mg-Ag alloys *European Cells & Materials* 25 (25) 2013: pp. 284 – 298.
25. **Rogal, L., Kania, A., Berent, K., Janus, K., Dobrzyn, L.** Microstructure and Mechanical Properties of Mg–Zn–RE–Zr Alloy After Thixoforming *Journal of Materials Research and Technology* 8 (1) 2019: pp. 1121 – 1131. https://doi.org/10.1016/j.jmrt.2018.09.002